Journal of Biomechanical Science and Engineering

Vol. 6, No. 4, 2011

Numerical Analysis of One-dimensional Mathematical Model of Blood Flow to Reproduce Fundamental Pulse Wave Measurement for Scientific Verification of Pulse Diagnosis*

Atsushi SHIRAI**, Tsutomu NAKANISHI** and Toshiyuki HAYASE**

**Institute of Fluid Science, Tohoku University,

2-1-1, Katahira, Aoba-ku, Sendai 980-8577, Japan

E-mail: shirai@ifs.tohoku.ac.jp

Abstract

Pulse diagnosis in traditional Chinese medicine is said to be able to detect not only illness but also decline of health in the patients from tactile sense of the pulse in the radial artery at the wrists. This diagnosis, however, is not supported by concrete scientific evidence. The authors have proposed a non-linear spring model of subcutaneous tissue on the radial artery and one-dimensional arterial blood flow model in an arm for the purpose of scientific verification of the pulse diagnosis. They performed, in the former study, a numerical experiment with this mathematical model in which the radial artery was indented in a stepwise manner by a pressure sensor, which extract the fundamental mechanism of the pulse diagnosis, to validate the subcutaneous tissue model and to find the appropriate coefficient to fit the experimental result. They investigated, in this research, contribution of parameters of supply pressure of the blood and tube law of the artery on the change in the pressure pulse waves with the indentation steps with respect to mean value P_{oav} and amplitude ΔP_o of the pressure. It was shown that mean supply pressure affects both P_{oav} and ΔP_o, while amplitude of the supply pressure affects ΔP_o. It was also shown that profile of ΔP_o vs. distance of the indentation changes drastically as the artery becomes hard. Lastly, it was examined to reproduce the experimentally obtained pressure pulse waves during the indentation in their former work with the mathematical model by adjusting the parameters. The result showed better agreement than the former result, but it implied that ulnar artery had to be taken into consideration for quantitative fitting of the pulse waves to the range where the radial artery was nearly flattened by the indentation.

Key words: Pulse Diagnosis, Pressure Wave, Mathematical Model, Numerical Simulation, One-Dimensional Analysis

1. Introduction

Integrated medicine (IM) that combines complementary and alternative medicine (CAM), such as traditional Chinese medicine, Ayurveda or aromatherapy, with modern Western medicine has recently attracted our attention. Research on IM is being carried out with the expectation of health maintenance, a decrease of medical expenses by prevention, early stage detection of diseases and perfect recovery from disease. It is hoped that

*Received 14 Jan., 2011 (No. 11-0034)
[DOI: 10.1299/jbse.6.330]

custom-made medical treatment based on individual patients' conditions can be realized.

Traditional Chinese medicine, represented by herbal medicine, acupuncture or moxibustion, is a well-known CAM. Pulse diagnosis is also a traditional Chinese medical technique. In the pulse diagnosis, a doctor places his fingers at both wrists of a patient to indent the radial arteries with various indentation patterns and diagnoses his/her diseases from the tactile sense of the pulse detected by the fingers. This is a simple and non-invasive technique and is said to be able to diagnose not only the diseases but also the patient's physical condition or presence of latent disease. The pulse diagnosis has been established with accumulated experiences of the doctors, and thus, neither scientific evidence of the diagnosis nor rigorous quantitative guideline for the diagnosis exist but qualitative image of tactile sense of the pulse waves specific to diseases. So, various researches have been performed on the objectification of the diagnosis[(1)-(5)]. In those researches, the pulse waves of the patients were measured by an applanation tonometry or a photoelectro-plethysmograph focusing on finding significant characteristics on the pulse waves for a specific disease and giving interpretation on them from medical point of view, but mechanism of the pulse diagnosis, i.e. cause-and-effect relationship between diseases and change in the waveform, was left unknown. This is an issue in integrating the pulse diagnosis to the modern Western medicine. Then, numerical simulation is a powerful tool for the fundamental understanding of the mechanism and analytical verification of the pulse diagnosis, because the mathematical model is grounded on rigorous physical laws.

Since blood flow is pulsatile by the heartbeat, some change in the circuit theoretically appears on the waveform of the pulsation by considering the blood circulatory system as a hydraulic circuit. For example, Konno et al.[(6)] examined the change of the waveform in their experimental research on the pulsatile flow in a closed circuit. For the investigation of the propagation or reflection of the pressure pulse waves, mathematical models of arterial vasculature have been proposed and numerical simulations have been performed[(7)-(10)]. In those researches, blood flow was expressed in one dimension, and the blood flow and the propagation of the pressure waves were solved simultaneously with deformation of the vessels under the physiological condition. The artery, however, has to be indented to reproduce the pulse diagnosis, because the authors have expected that essence of the diagnosis is in the change in the pulse waves by the indentation. For this purpose, we have to take into consideration the subcutaneous tissue between the radial artery and the finger. The authors proposed a non-linear spring model of subcutaneous tissue on the radial artery and one-dimensional blood flow in the artery of an arm to reproduce indentation of the radial artery by a finger[(11)]. They also developed an experimental setup to press down a pressure sensor against the radial artery at the wrist, and performed an experiment in which the radial artery was indented stepwise by a pressure sensor, which extracted the fundamental mechanism of the pulse diagnosis, to measure the change in the pressure pulse waves with the indentation steps. Quantitative agreement of the numerical and the experimental results is a necessary condition for the numerical reproduction of the pulse diagnosis and further investigation on the diagnosis. They then numerically reproduced the indentation experiment with the mathematical model to validate the subcutaneous tissue model and to find the appropriate parameter to fit the experimental result, and concluded that supply pressure and physical characteristics of the artery had to be adjusted for the quantitative agreement.

Therefore, in the present paper, the authors performed the numerical experiment to examine the contribution of the parameters of supply pressure of the blood and tube law of the artery to the change in the pressure pulse waves with the indentation steps with respect to the mean value and amplitude of the pressure, and lastly to verify their contribution to the pressure pulse waves detected by the sensor, parameters were adjusted to fit the numerical result with the experimental result.

Nomenclatures

$A(x)$: Cross-sectional area of artery at axial position x [m^2]
$A_0(x)$: Cross-sectional area of artery at axial position x at ϕ = 13.3 kPa [m^2]
$A_C(x)$: Cross-sectional area of artery at the inflection point of the tube law [m^2]
C_v: Capacitance of venous system [m^3/Pa]
$D(x)$: Peripheral length of artery at axial position x [m]
dy: Local displacement of arterial wall under pressure sensor [m]
dy_a: Time-averaged displacement of arterial wall under the center of pressure sensor [m]
dy_{av}: Mean displacement of arterial wall under pressure sensor [m]
f_t: Resistance coefficient of artery (= $\lambda/4$)
$P(x)$: Inner pressure of artery at axial position x [Pa]
P_E: Pressure at downstream end of artery [Pa]
$P_e(x)$: External pressure of artery at axial position x [Pa]
P_o: Pressure measured by pressure sensor [Pa]
P_{sav}: Mean supply pressure [Pa]
ΔP_o: Amplitude of pulsation pressure [Pa]
ΔP_s: Amplitude of supply pressure [Pa]
P_{ra}: Pressure in right atrium [Pa]
P_v: Venous pressure [Pa]
$Q(x)$: Flow rate of blood in artery at axial position x (= $A(x)u(x)$) [m^3/s]
Q_d: Flow rate of blood at downstream end of artery [m^3/s]
Q_{vi}: Flow rate of blood into vein [m^3/s]
Q_{vo}: Flow rate of blood out of vein [m^3/s]
$Re_x(x)$: Local Reynolds number in artery at axial position x (= $u(x)(A(x)/w(x))/\nu$)
R_m: Flow resistance in microvasculature [Pa·s/m^3]
R_v: Flow resistance in vein [Pa·s/m^3]
T: Tension of arterial wall in axial direction [N/m]
t: Time [s]
Δt: Time step for computation [s]
$u(x)$: Mean flow velocity of blood in artery at axial position x [m^3/s]
$w(x)$: Width of artery at axial position x when its cross section is assumed to be rectangle [m]
x: Axial position of artery from its upstream end [m]
Y: Displacement of pressure sensor [m]
$y(x)$: Height of artery from its center at axial position x when its cross section is assumed to be rectangle [m]
γ: Damping coefficient to the change in cross-sectional area of artery [Pa·s/m^2]
λ: Friction coefficient of pipe
ν: Kinematic viscosity of blood [m^2/s]
ρ: Density of blood [kg/m^3]
ϕ: Tube law [Pa]
ϕ_0: Transmural pressure (= $P - P_e$) at A/A_0 = 1 [Pa]

2. Method

In this section, measurement of pressure pulse waves by a pressure sensor and mathematical model to numerically reproduce the measurement are briefly explained. See Refs. (3) and (11) for the details.

2.1 Measurement of Pressure Pulse Waves by Pressure Sensor

Figure 1 shows the experimental setup for the measurement of pressure pulse waves in the radial artery at the wrist[11]. The pressure sensor moves vertically by the screw to indent

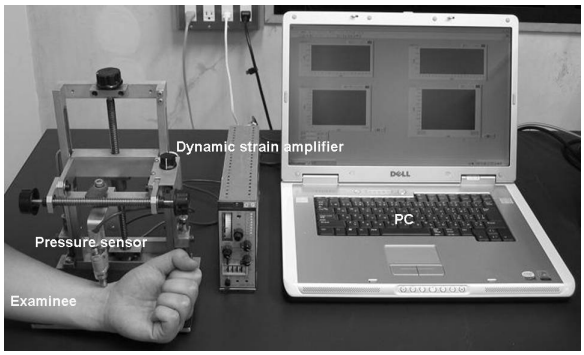

Fig. 1 Experimental setup for measurement of pulse waves[11].

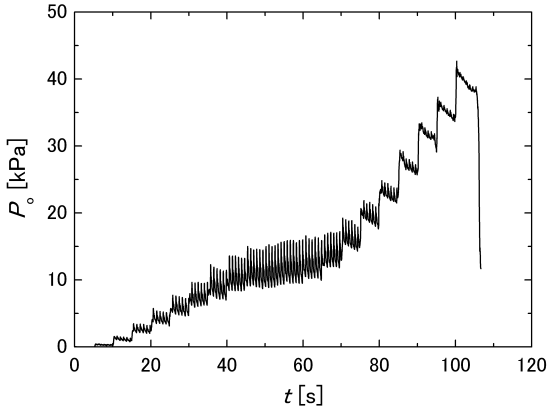

Fig. 2 Measured pressure waves P_o during the indentation[11].

the radial artery. The signal from the sensor was stored in a PC via a low-pass filter of 1 kHz of the strain amplifier and an A/D converter.

In the experiment, the pressure sensor was set at the position where pulsation was detected most clearly on the radial artery of a healthy 24 y.o. male volunteer, and measurement of the pulse waves was performed by the following steps, following the ethics regulation of Tohoku University and under the supervision of a medical doctor;

1: Displacement of the pressure sensor Y is set to 0 mm at the point the sensor touches wrist of the volunteer:
2: Press the sensor 0.5 mm down on the wrist and hold for 5 s to measure the pressure pulse waves.
3: Repeat step #2 until Y reaches 10 mm or the volunteer feels pain.

Figure 2 shows an example of the measured pressure pulse waves P_o. Here, each indentation period is not exactly 5 s because the screw was rotated by hand for the safety of the volunteer. The mean value of P_o in each indentation step correlates with physical characteristics of skin, subcutaneous tissue, blood vessel and mean blood pressure. Amplitude of the pulsation of P_o correlates with the pulsation of the blood flow. The mean value of P_o denoted as P_{oav} in the following has a non-linear profile with respect to indentation having an inflection point. The amplitude denoted as ΔP_o has the maximum around the inflection point of P_{oav}. This profile matches the principle of the applanation tonometry[12]. That is, pressure pulse waves in a cylindrical blood vessel that propagate outward are the balance of the inner pressure and radial projection of circumferential tension of the vessel wall. When the blood vessel is pressed between two flat surfaces, the circumferential tension can be ignored in the flattened area for the pulsatile inner pressure to directly propagate through that area. If the vessel is pressed more, blood flow itself ceases and the pulsation disappears. In this figure, pulsation of the blood flow is still observed in the range of $t \geq 100$ s where Y reaches 10.0 mm. This implies that the blood

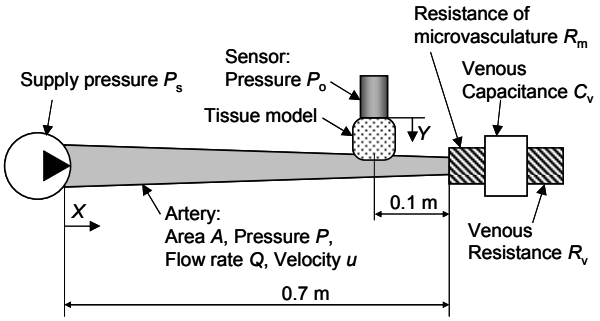

Fig. 3 Schematic of mathematical model.

flow was not fully ceased by the pressure sensor. The data shown in Fig. 2 is used for the comparison with the numerical results in the following.

2.2 Mathematical Model of Measurement of Pressure Pulse waves

Figure 3 shows a schematic of the mathematical model. This model is based on the collapsible tube model derived by Hayashi et al.[13]. In this research, we treated the series of subclavian artery, axillary artery, brachial artery and radial artery, neglecting the ulnar artery for the sake of simplicity. The arteries were assumed to be a tapered collapsible tube with a length of 700 mm. The inlet radius of the collapsible tube was 4.23 mm and the outlet radius was 1.74 mm, corresponding to those of the subclavian and radial arteries, respectively[14]. The linear resistance of the microvasculature, and the venous capacitance and the resistance of the Windkessel model were connected to the downstream end of the artery.

Blood was considered to be an incompressible Newtonian fluid with a density ρ of 1,050 kg/m^3 [15] and a kinematic viscosity ν of 3.8×10^{-6} m^2/s [16]. One-dimensional equation of momentum and continuity of blood in the artery are expressed as follows[13]:

$$\frac{1}{A}\frac{\partial Q}{\partial t}-\frac{Q}{A^2}\frac{\partial A}{\partial t}+\frac{Q}{A^2}\frac{\partial Q}{\partial x}-\frac{Q^2}{A^3}\frac{\partial A}{\partial x}=-\frac{1}{\rho}\frac{\partial P}{\partial x}-\frac{1}{2}f_t\frac{Q|Q|}{A^3}D\,, \tag{1}$$

$$\frac{\partial A}{\partial t}+\frac{\partial Q}{\partial x}=0\,. \tag{2}$$

where drag coefficient f_t is given as follows by the local Reynolsd number Re_x:

$$f_t=\frac{\lambda}{4}=\begin{cases}16/Re_x & (Re_x\le 1{,}067)\\ 0.015 & (Re_x>1{,}067)\end{cases}. \tag{3}$$

Here, friction coefficient λ of a pipe with a rough surface was $64/Re_x$ for the laminar flow region and was approximated by 0.06 in the turbulent flow region for the sake of simplicity[17].

To describe deformation of the collapsible tube, the initial cross section of the tapered collapsible tube was assumed to be a square whose cross-sectional area was same as that of the tube at all axial positions, i.e., both height y and width w of the tube were 7.50 mm at the inlet and 3.08 mm at the outlet. The width w was fixed along the collapsible tube and only the height y was changed to describe the deformation of the tube. Cross-sectional area A of the tube at arbitrary axial position x was expressed as A_0 when transmural pressure P–P_e was 13.3 kPa[18]. Force equilibrium acting on the tube wall in the normal direction to the wall was expressed as[13]

$$T\frac{\partial^2 y}{\partial x^2}=P_e-P+\phi\left(\frac{A}{A_0}\right)+\gamma\frac{\partial A}{\partial t}\,, \tag{4}$$

where T was approximated to be 130 N/m neglecting the variation of the tension, e.g. 107 N/m for the brachial artery and 138 N/m for the radial artery, because the series of the arteries was modeled as a tapered collapsible tube in this research[11].

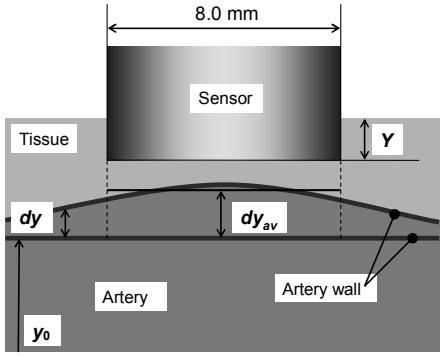

Fig. 4 Schematic of deformation of arterial wall and compression of subcutaneous tissue.

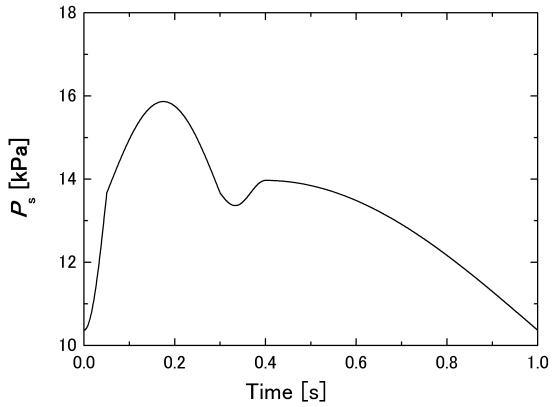

Fig. 5 Waveform of supply pressure P_s.

The third term of the right-hand side of Eq. (4) is the tube law of the artery. The tube law ϕ is the relationship between transmural pressure $P–P_e$ and the cross-sectional area A of the tube to represent stiffness of the blood vessel. The tube law introduced in the former researches on propagation and reflection of the pulse waves was based on the Laplace's law[7]-[10]. This model, as Olufsen mentioned[7], has a property that the area becomes infinite at a finite transmural pressure. In contrast, Shimizu and Ryumae[18] presented a tube law based on experimental data of canine carotid artery and femoral artery, which reproduces stiffening of the artery in the positive transmural pressure range. The authors introduced this model expressed as follows assuming human arteries have qualitatively the similar tendency as the canine arteries:

$$\phi\left(\frac{A}{A_0}\right)=\frac{\phi_0}{1+C_1-C_2}\left[\left(\frac{A}{A_0}\right)^{n_1}+C_1\frac{A}{A_0}-C_2\right] \quad \text{for } \frac{A_c}{A_0}\le\frac{A}{A_0}$$
$$\phi\left(\frac{A}{A_0}\right)=\phi_0\left[C_3\left(\frac{A-A_c}{A_0}\right)^{n_2}+C_4\frac{A-A_c}{A_0}+C_5\right] \quad \text{for } 0<\frac{A}{A_0}\le\frac{A_c}{A_0} \tag{5}$$

where the parameters are as follows: ϕ_0 = 13.3 kPa, C_1 = 0.1 and C_2 = 0.05. The A_C is the cross-sectional area at the connecting point of the two equations of Eq. (5), and C_3, C_4 and C_5 were determined to smoothly connect the two equations and the first differentiation at $A = A_C$. In this research, the gradient of ϕ at A/A_0 = 1.0 was doubled from the original model[18] and the absolute value of transmural pressure at A/A_0 = 0.0 was assumed to be twice of the mean blood pressure13.3 kPa (100 mmHg), considering the fact that Young's moduli of the canine aorta and the human radial artery are 0.43 MPa and 0.8 MPa, respectively[14], [19], and the fact that blood could not be stopped by an external pressure more than three times the mean blood pressure as shown in Fig. 2. Consequently, the parameters were determined as n_1 = 5, n_2 = 6, A_c/A_0 = 0.3, and ϕ = -26.6 kPa at A/A_0 = 0.

Here, the Young's modulus of human radial artery was compromised to be compared with that of canine aorta as the representative of canine arteries due to limitation of available data, though it should normally be compared with that of canine carotid artery or femoral artery with which the tube law was presented. The Young's modulus correlates with the gradient of ϕ at $A/A_0 = 1.0$, and is larger in peripheral arteries than central arteries[14]. The determined parameters, however, were used as the reference values and contribution of the Young's modulus to the pressure pulse waves was discussed in section 3.2.

The forth term of the right-hand side of Eq. (4) is viscous resistance to the change in cross-sectional area of the artery by the surrounding tissue. The damping coefficient γ against the change in the cross-sectional area of the artery was obtained as 2.5×10^8 Pa·s/m^2 from experimental data of loss of elastic coefficient of the canine artery[20]. However, since this value was so big for stable computation that we compromised by giving the largest coefficient $\gamma = 2.5\times10^7$ Pa·s/m^2 among the range of stable computation. The microvasculature was approximated by a linear resistance with the resistance coefficient R_m of 4.3×10^9 Pa·s/m^3, and the venous system was approximated by the Windkessel model with the resistance coefficient R_v of 8.3×10^8 Pa·s/m^3 and capacitance C_v of 1.95×10^{-9} m^3/Pa[11].

We also have to take into consideration the transfer characteristics of the subcutaneous tissue between the pressure sensor and the arterial vessel wall to reproduce the indentation experiment explained in section 2.1. The relationship between the compression of the tissue by the pressure sensor and vessel wall, and repulsion pressure of the tissue to artery P_e is given as

$$P_e = a(Y + dy_{av})^2, \tag{6}$$

where $a = 10.0\times10^8$ Pa/m^2 is the coefficient of the subcutaneous tissue model[11], and dy_{av} is the mean value of dy under the center of the sensor as shown in Fig. 4, where dy is displacement of the artery wall from its steady state y_0. Here, both Y and dy_{av} are positive in the direction of compression of the tissue, and pressure detected by the sensor P_o equals the external pressure of the artery P_e according to the principle of reaction.

Numerical simulation was performed by the 4th-order Runge-Kutta method with the time step of $\Delta t = 10^{-7}$ s to solve pulsatile blood flow and deformation of blood vessel simultaneously. Here, as for the supply pressure, the waveform shown in Fig. 5 was determined from the measured data at the brachial artery[21] as the mean value $P_{sav} = 13.3$ kPa (100 mmHg) and amplitude $\Delta P_s = 5.5$ kPa (41.25 mmHg)[11]. The artery was divided into 284 cells with non-uniform meshing so that the mesh under the pressure sensor was accumulated to 16 cells[11].

3. Results and Discussion

In the following sections, the indentation experiment introduced in section 2.1 was numerically reproduced with the mathematical model to investigate the contribution of the supply pressure of the blood and the tube law of the artery to the changes in mean value P_{oav} and amplitude ΔP_o of the pressure P_o detected by the sensor with the indentation steps. Lastly to verify their contribution to the pressure pulse waves detected by the sensor, it was examined to reproduce the pressure pulse waves measured in the indentation experiment with the mathematical model by adjusting the parameters.

3.1 Effect of Supply Pressure

In this section, the contribution of the supply pressure P_s at the upstream end of the collapsible tube to P_{oav} and ΔP_o was examined numerically. For this purpose, mean value P_{sav} and amplitude of pulsation ΔP_s of P_s were changed from the original values, $P_{sav} = 13.3$ kPa and $\Delta P_s = 5.5$ kPa, keeping the waveform shown in Fig. 5. In the classification of blood pressure range put forwarded by the Japan Society of Hypertension, normal ranges of the systolic pressure, diastolic pressure and amplitude of the pulsation are less than 140 mmHg,

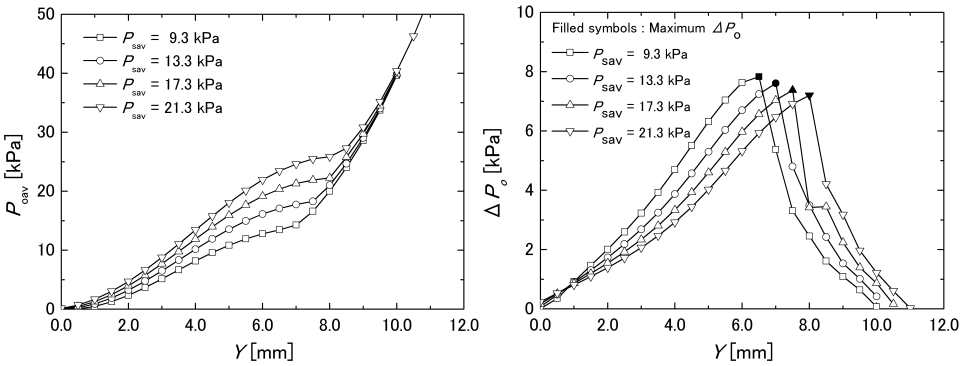

(a) Mean pressure P_{oav}. (b) Amplitude of pulsation ΔP_o.

Fig. 6 Numerical reproduction of indentation experiment with four mean supply pressure P_{sav}.

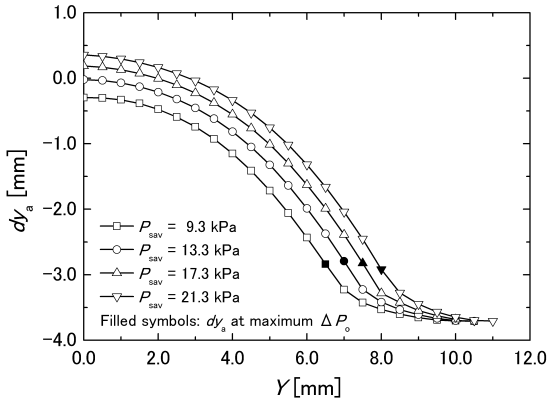

Fig. 7 Relationship between indentation Y and time-averaged displacement of vessel wall under the center of the sensor dy_a.

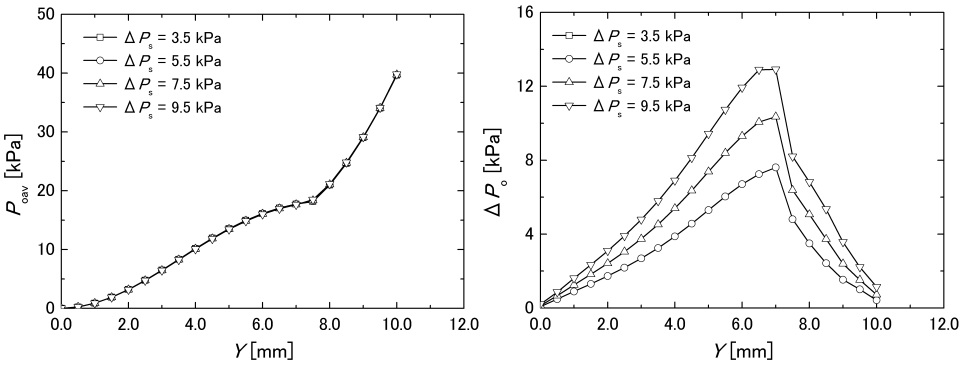

(a) Mean pressure P_{oav}. (b) Amplitude of pulsation ΔP_o.

Fig. 8 Numerical reproduction of indentation experiment with four amplitude of supply pressure ΔP_s.

less than 90 mmHg, and 30 to 50 mmHg, respectively[22]. Therefore, mean pressure of 13.3 kPa (100 mmHg) and amplitude of 5.5 kPa (41.3 mmHg) is in the normal range, respectively.

First, P_{sav} was chosen from among 9.3, 13.3, 17.3 and 21.3 kPa while keeping the amplitude ΔP_s = 5.5 kPa. Figures 6(a) and 6(b) show the numerically obtained relationship between Y and P_{oav}, and Y and ΔP_o, respectively. In Fig. 6(a), P_{oav} is higher for high P_{sav} in the range $Y < 8.0$ mm. This is explained as follows: Figure 7 shows the relationship between Y and time-averaged displacement of the vessel wall under the center of the sensor dy_a. We can say from this figure that dy_a increases with the increase in the inner pressure P_{sav} at a fixed Y to compress the subcutaneous tissue from inside the arm by the vessel, and thus,

P_{oav}, which equals the time-averaged value of P_e in Eq. (6), increases with the increase in P_{sav} since dy_{av} increases with the increase in dy_a. On the contrary, the difference in P_{oav} between high and low P_{sav} becomes small in the range of $Y \geq 8.0$ mm, and the lines in Fig. 6(a) follow the tube law in negative ϕ.

In Fig. 6(b), Y which gives the maximum ΔP_o increases with the increase in P_{sav}. This is explained as follows: Filled symbols in Fig. 7 correlate with those in Fig. 6(b). In Fig. 7, dy_a which gives the maximum ΔP_o is almost constant and A/A_0 was about 0.15 independent of P_{sav} while dy_a at $Y = 0$ mm increases with P_{sav}. Therefore, displacement of the sensor Y to press the vessel wall down to this point increases with the increase in P_{sav}. Here, the peak value of ΔP_o slightly decreases with the increase in Y. This implies that, though the precise mechanism is unknown, the peak value decreases as the subcutaneous tissue is compressed.

Next, ΔP_s was chosen from among 3.5, 5.5, 7.5 and 9.5 kPa while keeping $P_{sav} = 13.3$ kPa. Figures 8(a) and 8(b) show the numerically obtained relationship between Y and P_{oav}, and Y and ΔP_o, respectively. In Fig. 8(a), P_{oav} is not influenced by ΔP_s. This is because that, since ϕ correlates with the supply pressure P_s, mean value of A/A_0 at each Y does not change with ΔP_s so far as P_{sav} is fixed. On the contrary, as shown in Fig. 8(b), ΔP_o increases with the increase in ΔP_s, and the value of ΔP_o at each Y is nearly proportional to ΔP_s. This is because that amplitude of A/A_0 becomes large with the increase in ΔP_s.

Here, it is generally said to be low blood pressure when systolic blood pressure is less than 100 mmHg, and it is said to be high blood pressure when systolic and diastolic blood pressures are 140 mmHg or more and 90 mmHg or more, respectively[22]. When $P_{sav} = 9.3$ kPa, systolic blood pressure at $\Delta P_s = 3.5$ kPa is 87 mmHg and is determined to be in the low blood pressure. When $P_{sav} = 21.3$ kPa, systolic and diastolic blood pressures at $\Delta P_s = 11.5$ kPa are 207 mmHg and 136 mmHg, respectively, and it is classified to be in the serious high blood pressure in which systolic and diastolic blood pressures are 180 mmHg or more and 110 mmHg or more, respectively. Therefore, the combination of P_{sav} and ΔP_s covers from the low blood pressure to the high blood pressure.

3.2 Effect of Tube Law of Artery

Although the tube law is an important parameter which expresses the stiffness of the arterial vessel wall, there have been few attempts to observe it directly. Many research studies have been performed to observe the relationship between transmural pressure and the diameter of an artery to predict the physical characteristics of the vessel wall, and a non-dimensional parameter named the stiffness parameter β has been introduced[23]. The relationship between inner pressure P and radius R of an artery under the physiological condition is expressed as

$$\ln\left(\frac{P}{P_b}\right) = \beta\left(\frac{R}{R_b} - 1\right), \tag{7}$$

where P_b is an arbitrary inner pressure (generally $P_b = 13.3$ kPa), and R_b is the radius at $P = P_b$. Assuming that the cross section of the artery is a circle under the physiological conditions, we can obtain β from the tube law as

$$\beta = \frac{2}{P_b}\frac{dP}{d(A/A_0)}\bigg|_{A/A_0=1}. \tag{8}$$

The stiffness parameter of human arteries is known to increase with aging or progression of diseases[23]. In this section, the influence of the stiffness of the artery on the measured pressure pulse waves is examined numerically. For this purpose, a parameter of the tube law n_1 was chosen from among 2, 3, 6 and 12, taking into consideration the stiffness parameter obtained with the carotid and femoral arteries of human[24]. The correspondence of n_1 and β of the above-mentioned n_1 is shown in Table 1 together with that of the original $n_1 = 5$. The n_1 influences the gradient of the tube law at $A/A_0 = 1$, the

Table 1 Correspondence table between parameter n_1 of tube law and stiffness parameter β.

n_1	2	3	5	6	12
β	4.0	5.9	9.7	11.6	23.0

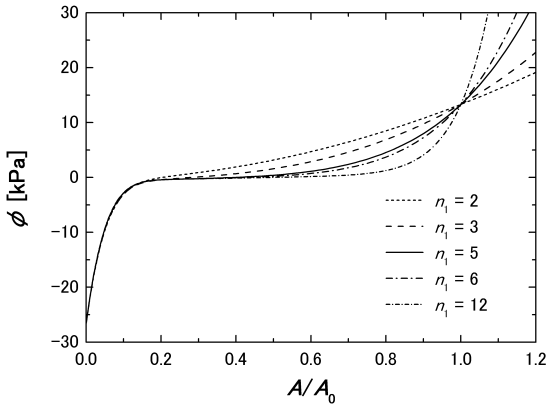

Fig. 9 Variation of tube law by n_1.

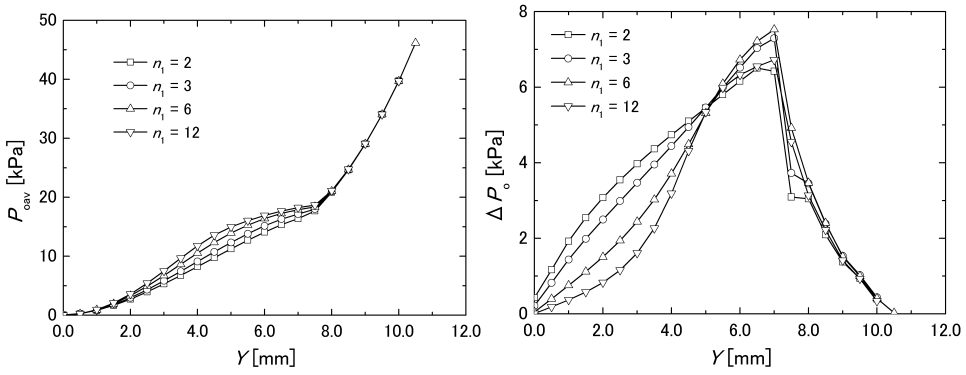

(a) Mean pressure P_{oav}. (b) Amplitude of pulsation ΔP_o.

Fig. 10 Numerical reproduction of indentation experiment with four tube laws.

artery in the physiological range of the transmural pressure, 10.5 kPa < ϕ < 16.0 kPa, becoming hard as n_1 increases, as shown in Fig. 9. Here, the authors compromised by giving almost the same tube law in the range of ϕ < 0.0 kPa (A/A_0 < 0.2) because they have neither measurement data of the tube law out of the range of blood pressure nor knowledge of the influence of such factors as aging or arteriosclerosis on the tube law. The gradient of the tube law is decreased as the increase in n_1 in the positive range of small transmural pressure ϕ. This represents the cross section A decreases drastically with a small decrease in ϕ.

Figures 10(a) and 10(b) show the numerically obtained relationship between Y and P_{oav}, and Y and ΔP_o, respectively, for the four variations of n_1. Here it was confirmed that the displacement of the artery under the center of the pressure sensor $|dy_a|$ was smaller for large n_1 in the range of Y < 8 mm. Since dy_a is negative in the direction of indentation, measured pressure P_o becomes larger for large n_1 as understood from Eq. (6). Therefore, P_{oav} is large for large n_1, as shown in Fig. 10(a) in the range of Y < 8 mm, and thus, it can be said that a soft artery reduces the measured mean pressure. On the contrary, P_{oav} in the range of $Y \geq 8$ mm is almost the same independent of n_1 and follows the tube law in the negative ϕ region of A/A_0 < 0.15.

The profile of the relationship between Y and ΔP_o in Fig. 10(b) drastically changes in the range of $Y \leq 5$ mm, i.e., it is convex-up for small n_1 but becomes convex-down with the

Table 2 Parameters which best fit the experimental data.

a [Pa/m^2]	P_{sav} [kPa]	ΔP_s [kPa]	n_1
11.0×10^8	8.3	4.5	8

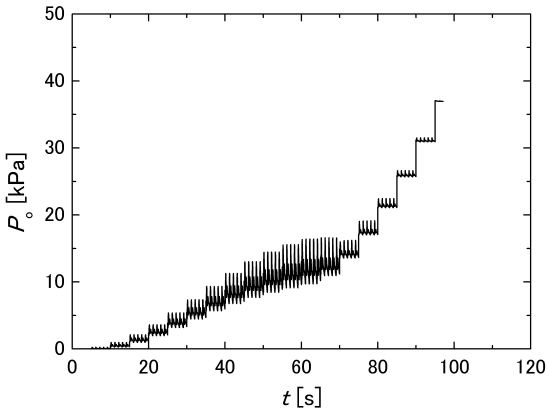

Fig. 11 Pressure pulse waves obtained by numerical simulation with the parameters shown in Table 2.

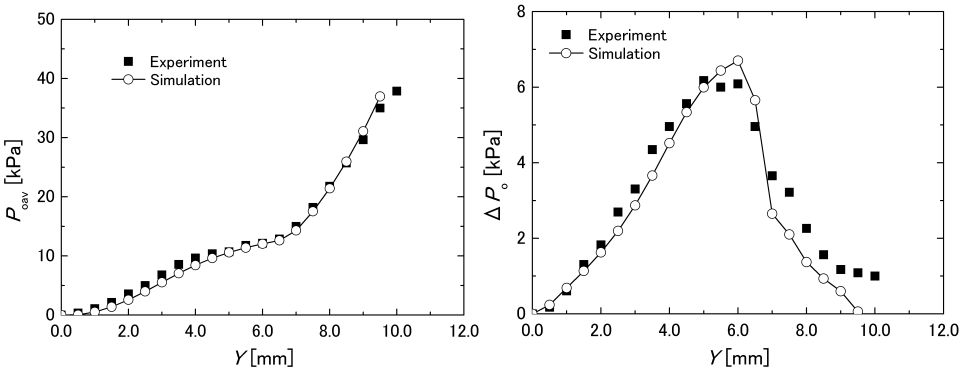

(a) Mean pressure P_{oav}. (b) Amplitude of pulsation ΔP_o.

Fig. 12 Comparison of numerical result with experimental data.

increase in n_1. This is because, as seen in Fig. 9, in the range of small Y, change in the cross-sectional area for a certain amplitude of ϕ is small for large n_1 owing to difference in the gradient of ϕ around $A/A_0 = 1$. This difference in the profile can be an index to predict the stiffness parameter. Here, the reason for the kink at $Y = 7.5$ mm is unknown.

3.3 Reproduction of Experimental Data

To verify the contribution of the parameters of the subcutaneous tissue model[11], the supply pressure and the tube law to the changes in P_{oav} and ΔP_o, numerical reproduction of the experimentally obtained pressure pulse waves shown in Fig. 2 was examined. The parameters determined to best fit the experimental result are listed in Table 2, and the resultant numerically obtained pressure pulse waves are shown in Fig. 11. The relationship between Y and P_{oav}, and Y and ΔP_o are shown in Fig. 12(a) and 12(b), respectively. Both P_{oav} and ΔP_o show better agreement to the experimental data than the former result[11]. In Fig. 12(b), however, the discrepancy in ΔP_o in the range of $Y \geq 7$ mm is relatively larger than that in the range of $Y < 7$ mm. This is considered to be because pressure pulsation propagates backward to the collapsed radial artery via the ulnar artery and the palmar arch in addition to arbitrary determination of the tube law in the negative transmural pressure range.

4. Conclusions

A simple mathematical model of one-dimensional blood flow in the artery of an arm and the subcutaneous tissue on the radial artery was developed, while in a previous study, an experimental setup to press a pressure sensor against the radial artery at the wrist was designed for the purpose of collecting scientific evidence for pulse diagnosis[11]. An experiment to indent the radial artery in a stepwise manner by the pressure sensor was performed to measure the change in the pressure pulse waves with the indentation steps. The experiment was then numerically reproduced with a mathematical model, suggesting that the mathematical model has a potential to quantitatively reproduce the pulse diagnosis.

In the present study, contributions of parameters of the supply pressure of blood and the tube law of the artery to the changes in the mean value and amplitude of the pressure pulse waves when the pressure sensor was pressed down on the radial artery were examined using the mathematical model. Obtained results summarized in terms of the displacement Y of the sensor are enumerated as follows: (1) The mean pressure increased with the increase in mean supply pressure. However, it followed the tube law in the negative transmural pressure range after the artery was nearly collapsed by the sensor. The Y which gave the maximum amplitude of the pulsation increased and the peak value slightly decreased with the increase in the mean supply pressure. (2) The Y which gave the maximum amplitude of the pulsation did not change, but the amplitude increased nearly in proportion to the amplitude of the supply pressure. (3) The profile of the amplitude of pulsation in the range of $Y \leq 5$ mm drastically changed from convex-up to convex-down with the increase in n_1 of the tube law. This change in the profile is a possible index to predict the stiffness parameter of the artery.

It was examined to reproduce the pressure pulse waves measured in the indentation experiment with the mathematical model by adjusting parameters taking into consideration these results. It was suggested that pressure pulsation propagates backward to the collapsed radial artery via the ulnar artery and the palmar arch. Therefore, the authors are planning to extend the blood circulation system of an arm to take into consideration the blood perfusion through the ulnar artery.

Acknowledgements

A part of this research was performed with the support of the Sendai Area Knowledge Cluster Initiative (Stage II). The authors appreciate the helpful suggestions of Professor Shin-ichi Nitta, Associate Professor Hiroshi Kawada, Senior Assistant Professor Mitsuya Maruyama and Assistant Professor Satoshi Konno of Institute of Development, Aging and Cancer, Tohoku University, Dr. Takashi Seki of Tohoku University Hospital, and Associate Professor Makoto Ohta of Institute of Fluid Science, Tohoku University.

References

(1) Shirota, F., Mitsufuji, H., and Igarashi, H., Scientific Verification of Oriental Diagnoses, *Kampo Med.,* Vol. 22 (1972), pp. 201-209. (in Japanese)

(2) Takashima, M., Nagaya, K., Kikuna, T. and Matsuya, K., Development of new apparatus for oriental pulse diagnosis, *Kampo Med.*, Vol. 47 (1997), pp. 635-643. (in Japanese)

(3) Fujita, R., The study of pulse diagnosis (18th. Report) – improved photoelectroplethysmograph – (2nd. report), *Kampo Med.*, Vol. 28 (1977), pp. 81-84. (in Japanese)

(4) Onaka, M., Objectification of the pulse diagnosis by arterial tonometry, *Oriental Med. Pain Clinic*, Vol. 31 (2001), pp. 34-40. (in Japanese)

(5) Uebaba, K., O'rourke, M.F., Xu, F., Ishiyama, H., Amano, K. and Kasahara, H., Radial artery pulse wave analysis in assessment of cardiac function – Value of traditional pulse diagnosis –, *Eastern Med.*, Vol. 17, No. 2 (2001), pp. 1-13.

(6) Konno, S., Maruyama, M., Nitta, S., Takashima, M., Shiraishi, Y., Yambe, T., Ohta, M., Ryu, R., Narumi, K., Shirai, A., Hayase, T., and Yoshizawa, M., Effect of the blood flow of ulnar artery on radial artery pulse wave, *Transactions of the Japanese Society for Medical and Biological Engineering*, Vol. 44, Suppl. 1 (2006), pp. 592. (in Japanese)
(7) Olufsen, M.S., Structured tree outflow condition for blood flow in larger systemic arteries, *Am. J. Physiol. Heart Circ. Physiol.*, Vol. 276 (1999), pp. 257-268.
(8) Sherwin, S.J., Franke, V., Peiro, J. and Parker, K., One-dimensional modeling of a vascular network in space-time variables, *J. Eng. Math.*, Vol. 47 (2003), pp. 217-250.
(9) Vignon, I.E. and Taylor, C.A., Outflow boundary conditions for one-dimensional finite element modeling of blood flow and pressure waves in arteries, *Wave Motion*, Vol. 39 (2004), pp. 361-374.
(10) Alastruey, J., Parker, K.H., and Peiró, J., Analysing the pattern of pulse waves in arterial networks: a time-domain study, *J. Eng. Math.*, Vol. 64 (2009), pp. 331-351.
(11) Narumi, K., Nakanishi, T., Shirai, A., and Hayase, T., Development of One-Dimensional Mathematical Model for Validation of Pulse Diagnosis, *Trans. JSME*, Ser. B, Vol. 74, No. 737 (2008), pp.142-148. (in Japanese)
(12) Ohnaka, M., Investigation of Objective Evaluation of Pulse Diagnosis, *Oriental Medicine and The Pain Clinic*, Vol. 31 (2001), pp. 34-40. (in Japanese)
(13) Hayashi, S., Hayase, T., Shirai, A., and Maruyama, M., Numerical Simulation of Noninvasive Blood Pressure Measurement, *Trans. ASME, J. Biomech. Eng.*, Vol. 128 (2006), pp. 680-687.
(14) Wang, J.J., and Parker, K.H., Wave propagation in a model of the arterial circulation, *J. Biomech.*, Vol. 37 (2004), pp. 457-470.
(15) Hershey, D., and Smolin, R., Linear regime transition for blood flow in tubes, *Biorheology*, Vol. 4 (1966), pp. 61-67.
(16) Okino, H., Sugawara, M., and Matsuo, H. ed., *Dynamics and Fundamental Measurement of Cardiovascular System*, Kodan-sha (1980), pp. 125-132. (in Japanese)
(17) Nikurades, J., Gesetzmässigkeit der tuburenten Strömung in glatten Rohren, *Forsch. Abr. Ing. –Wes.*, 356 (1932).
(18) Shimizu, M. and Ryumae, S., Model of Arterial Volume Change under the Cuff during Blood Pressure Measurement, *Japanese Journal of Medical Electronics and Biological Engineering*, Vol. 30, No. 4 (1992), pp. 267-275. (in Japanese)
(19) Oka, S., *Biorheology*, Syokabo Publishing Co. Ltd. (1984). (in Japanese)
(20) Bergel, D.H., The Dynamic Elastic Properties of Arterial Wall, *J. Physiol.*, Vol. 156 (1961), pp. 458-469.
(21) Yoshimura, M., Mishima, Y., Hattori, K., and Maeda, K. ed., *Clinical Pulse Wave Decipherment Course I*, Kanehara & Co., Ltd. (1994). (in Japanese)
(22) Ozawa, T., Editorial: Clinical measurement of pulse pressure, *Arterial Stiffness No. 8*, Medical View Co. Ltd. (2005). (in Japanese)
(23) Hayashi, K., *Biomechanics*, Corona Publishing Co. Ltd. (2000). (in Japanese)
(24) Kawasaki, T., Sasayama, S., Yagi, S., Asakawa, T., and Hirai, T., Non-invasive assessment of the age related changes in stiffness of major branches of the human arteries, *Cardiovasc. Res.*, Vol. 21 (1987), pp. 678-687.